Fast simulation of ultrasound images from a CT volume.

Jean-Louis Dillenseger, Soizic Laguitton, Eric Delabrousse

▶ To cite this version:

Fast Simulation of Ultrasound Images from a CT volume

Jean-Louis Dillenseger*,**   Soizic Laguitton*,**   Éric Delabrousse***,****

From:

* INSERM, U642, Rennes, F-35000, France;

** Université de Rennes 1, LTSI, Rennes, F-35000, France;

*** INSERM, U556, Lyon, F-69003 France;

**** Université Claude Bernard Lyon 1, Lyon, F-69000 France.

Corresponding author:

Jean-Louis Dillenseger

Laboratoire Traitement du Signal et de l'Image,

INSERM U642, Université de Rennes I,

Campus de Beaulieu, 35042 Rennes Cedex, France.

tel: +33 (0)2 23 23 55 78 fax: +33 (0)2 23 23 69 17

email: Jean-Louis.Dillenseger@univ-rennes1.fr

Abstract

The goal of our work is to propose a fast ultrasound image simulation from CT volumes. This method is based on a model elaborated by Bamber and Dickinson that predict the appearance and properties of a B-Scan ultrasound image from the distribution of point scatterers. We propose to extend this model for the standard medical ultrasound image simulation by taking into account the acoustical tissue properties (scatterer distribution) and the geometry and the specifications of the ultrasound probe (circular probe, number and size of transducers, US pulse frequency and bandwidth, etc.). Simulations have been obtained in a fairly fast computation speed and qualitatively they present most of the real ultrasound image characteristics.

Key Words

Acknowledgements

1 Introduction

For most surgical procedures, the imaging techniques used to establish the preoperative planning are different to those used during the per-operative surgical treatment. This is the case for example, for some minimal invasive percutaneous surgical acts in hepatology (hepato-cellular carcinoma ablation by radiofrequency (RF) or high intensity ultrasound, US) or in urology (renal puncture or radiofrequency treatment) where needle-like tools are introduced in the patient's body to a specific target. In these cases, the preoperative planning is established on 3D images (CT, MRI) which provide high resolution anatomical information on the patient's case. In counterpart, the puncture is an US image guided surgical intervention. US is generally trickier to interpret. The connection between these two imaging techniques is

2

problematic in terms of information correlation and interpretation. A solution can be given by the simulation of US images from the preoperative 3D volumes and more specifically CT in our case.

Beyond this application example, the simulation of US images can have several uses in image guided surgery and also on other biomedical domains: US probe design [1, 2], model for US image characterization or segmentation purpose [3, 4], US image interpretation learning, simulators for medical training [5, 6],...

The objective of our study is the simulation of images provided by the classical US probes from CT 3D volumes. No direct relations between these two modalities exist. Our problem can be split into two stages: 1) the construction of tissue models from the CT scans information and 2) the US scans simulation itself from the tissue models and a modeled US system.

The first difficulty lies in the construction of tissue models from the CT scans information. The main aspect of an US image is provided by the speckle. Speckles come from the interference of the signal reflected by tissue micro-inhomogeneities (capillaries, tissues or blood cells, etc.). The micro-inhomogeneities size are below the resolution of the CT scan so speckle cannot been directly deducible from the CT data. Only the main tissues can be extracted from the data. However, some work has been done in US speckle analysis and modeling, mainly for tissue characterization purpose [7, 8, 9]. The outcomes of such work can be used to simulate the speckle spatial distribution for each extracted tissue.

Concerning the second stage, the simulation of US scans, two main approaches have been previously proposed:

- The simulation and modeling of the emitted field and the pulse-echo responses of the organs using linear acoustics. This is the case of Jensen's studies [1] where the organs are modeled using distribution of point scatterers. The US image is estimated by the simultaneous study of the transducers interference, the physical, spatial and temporal US field propagation and its interaction with the scatterers. The precision of this approach is obtained to the detriment of the computing time. For example, in 2000, Jensen reports on the results of a fast version of its algorithm. The computation of a 64x64 image simulation with 200,000 scatterers takes more than 3 hours [10].

- The direct prediction of the US image appearance from the single scatterers' contribution. The pioneer study has been proposed by Bamber and Dickinson [11]. It is based on the relation between the final produced US image appearance and the ultrasonic field/point scatterers' interaction. If this relation is assumed to be a single diffuse reflection, the image formation can be summarized as the convolution of a scatterers map by an ultrasonic field model. An image can so be build in the computation time of a simple image convolution. This technique has been validated by the simulation of high resolution US scans of small regions.

Our objective is to propose a fast US image simulation from preoperative CT volumes. More particularly we wish to simulate standard US scans with a high field of view like abdominal images. For a fast US image simulation, the model proposed by Bamber and Dickinson [11] seems to be the most appropriate. However, the main assumption of this method is that the US pulse and beam shape are assumed invariant. This assumption is only true within small regions and leads to limit the computation of the US images of these small regions.

In this paper, we extended Bamber and Dickinson's model to produce images simulated from standard probes. Two directions have been explored: 1) the construction of a tissue model from the CT scan information which is based on a model that directly described the spatial placement of point scatterers and 2) an US images generation process which adapts Bamber and Dickinson's model to the standard probe geometry and beam shape. Section 2 provides the basic features of the work: the Bamber and Dickinson's original model, the tissue modeling and the final US image generation. In section 3, the results of the simulation framework are presented and finally compared to real US images.

2 Methods

The starting data is an image (or a sub-volume) extracted from the 3D CT volume where the pixel (or voxel) size is known. The geometry and the characteristics of the US probe (circular probe, number and size of transducers, US pulse frequency, quality factor Q of the US pulse emission spectrum, etc.) are the input parameters.

2.1 Bamber and Dickinson's model

It is based on a linear modeling[1] of the properties of an ultrasonic signal reflected diffusely in an inhomogeneous medium. This model which derives from the wave equation, describes the signal as the integration of impulse responses:

$$I_{3D}(x,y,z) = \int \int \int H_{3D}(x,y,z,\alpha,\beta,\gamma) \cdot T(\alpha,\beta,\gamma) \cdot d\alpha \cdot d\beta \cdot d\gamma \qquad (1)$$

where I_{3D}, is the resulting 3D radiofrequency (RF) image; x the propagation direction (the axial direction) of the US wave; y and z its lateral and transverse directions; H_{3D}, the system impulse response or point spread function (PSF), i.e. the 3D RF image of a point; and T, a function describing the tissue echogenicity which depends directly on its acoustical impedance.

For a small region, the PSF H_{3D} can be assumed as invariant in space. Equation (1) can so be written as a convolution product:

$$I_{3D}(x,y,z) = (H_{3D} * T)(x,y,z) \qquad (2)$$

The PSF $H_{3D}(x,y,z)$ is generally modeled as a wave modulated by a Gaussian envelope:

$$H_{3D}(x,y,z) = e^{-\frac{1}{2}(\frac{x^2}{\sigma_{ax}^2} + \frac{y^2}{\sigma_{lat}^2} + \frac{z^2}{\sigma_{trans}^2})} \cos(2\pi f x) \qquad (3)$$

where f is the spatial pulse frequency; σ_{ax} stands for the pulse length and is directly related to the pulse emission spectrum bandwidth; σ_{lat} and σ_{trans} stand for respectively the pulse width and thickness and are directly related to the transducers geometry and size.

$T(x,y,z)$, the function describing the tissues echogenicity is given by [3]:

$$T(x,y,z) = \frac{1}{2Z_0} \frac{\partial^2 Z_{3D}}{\partial x^2}(x,y,z) \qquad (4)$$

where Z_0 is the acoustical impedance referential and $Z_{3D}(x,y,z)$ the tissue acoustical impedance.

---

[1] The model is linear because it uses Born's approximation to solve the wave propagation equation in inhomogeneous medium.

The radiofrequency image of a slice (a 2D scan) for a specific constant $z = z_0$ can be computed by (omitting $1/2Z_0$ for simplicity):

$$I(x,y) = I_{3D}(x,y,z_0) = (H_{3D} * \frac{\partial^2 Z_{3D}}{\partial x^2})(x,y,z_0) \tag{5}$$

I_B, the final simulated B-scan US image is obtained by an envelope detection of the RF image. This detection can be performed by:

$$I_B(x,y) = |I(x,y) + j \cdot Hilbert(I(x,y))| \tag{6}$$

where $Hilbert()$ is the Hilbert transform.

In their model, Bamber and Dickinson made the assumption of a space invariant PSF. This is true only with parallel wave propagation within small tissue regions.

2.2   Tissue modeling

In Equation 4, tissues are modeled by their acoustical impedances. On the CT image, a simple threshold based segmentation allows to form several tissue classes (bone, soft tissues, fat, blood and air). According to the classification, acoustical impedances are allocated to each image pixel.

However, the main part of a US image consists of a speckle pattern. Speckles come from the interference of the signal scattered by tissue micro-inhomogeneities (tissue cells, capillaries, blood cells, etc.) which are not directly deducible from the CT data. In the other simulators, these micro-inhomogeneities are generally simulated by randomly placed scatterers (see [10] for example). More recently, Laporte et al. [12] suggested to use the 1D marked regularity model of Cramblitt and Parker [7] and to extend it to higher dimensions. This model is based on the following scatterer function adapted to the 1D space domain:

$$s(x) = \sum_i a_i \delta(x - X_i) \tag{7}$$

where a_i and X_i denote the amplitude and the location of scatterer i. The inter-scatterer distances $d_i = X_{i+1} - X_i$ are independent and randomly distributed from a gamma distribution with shape and scale parameters α and β:

$$f(d) = \frac{d^{\alpha-1} \exp(-d/\beta)}{\Gamma(\alpha)\beta^\alpha} \qquad d, \alpha, \beta > 0 \tag{8}$$

where $\Gamma()$ is the Gamma function. The mean and variance of the inter-scatterer distances are $\overline{d} = \alpha\beta$ and $\sigma_d^2 = \alpha\beta^2 = \overline{d}^2/\alpha$. Thus the scatter model can be tuned in terms of density (the density is $1/\overline{d}$) and regularity (by varying the shape parameter α).

As suggested in [7], the amplitudes a_i were independently sampled from a log-normal distribution with mean 1 and variance 0.1.

The marked regularity model is able, by adjusting the density and the regularity parameters, to generate the scatterer processes that results in the RF amplitude distributions analyzed in the literature like Rayleigh, Rician or K distributions.

But this 1D model cannot be generalized in higher dimensions. However, Laporte et al. [12] suggest to map the 1D line segment onto the higher N-dimension spaces by using Hilbert filling curves, which are fractal curves in the N-dimensional spaces, because they tend to preserve locality.

In concrete terms, the construction of the acoustical impedance map used in Equation 4 follows this framework:

1. The segmentation of the CT slice (or sub-volume) pixels onto several tissue classes (bone, soft tissues, fat, blood and air) by simple thresholding.

2. The classified regions are not regular, but on the other hand Hilbert filling curves need to be constructed on square (or cubic) areas. In order to recover this regularity, we performed a spatial decomposition of the classified slice (or volume) by a quadtree (or octree) encoding. Each quadtree (or octree) terminal cell is representative of a regular homogeneous region.

3. The global tissues' acoustical impedance map is obtained by filling each terminal cell by the acoustical impedance related to the tissue.

4. The scatterer distribution is performed for each terminal cell, according to the following scheme:

(a) Scatterers are distributed on a line using the 1D marked regularity model (Equation 8) initialized by the density and regularity parameters related to the tissue.

(b) We used a fast Hilbert filling curves algorithm inspired by [13] to map the line carrying the scatterers generated by Cramblitt's model onto 2D or 3D spaces.

(c) On the obtained scatterers' 2D (or 3D) location, the scatterers' amplitudes are multiplied to the tissue acoustical impedance.

2.3 Model adaptation to abdominal US images

Several issues have to be taken into account when dealing with abdominal US: the probe is generally circular; the PSF has to be physically adapted to the probe geometry and emission spectrum (its shape depends directly on the propagation direction and on the beam shape which is not constant during the propagation); the high field of view leads also to resolution problems. The adaptation of Bamber's model has been performed in the following way [14]:

- Spatial geometry of a circular US probe. The abdominal US probes are circular with a different propagation direction for each transducer. However, Bamber's model assumed parallel wave propagation. A Cartesian/polar transform allows recovering a parallel propagation direction.

- Image resampling in order to respect Shannon's sampling theorem. The CT image voxel (or pixel) size (around 0.7 mm) is generally greater than the US wavelength (with a 1540 m/s ultrasound propagation speed in the human tissues and a 3.5 MHz pulse frequency, the wavelength is λ=c/f=0.44 mm). The PSF H_{3D} is directly related to the wavelength (cf. Equation 3). So, in order to respect Shannon's sampling theorem the transformed CT scan within the polar coordinate system has to be resampled by linear interpolation along the propagation axis.

- Probe geometric and spectral influence on the PSF. The probe pulse emission spectrum and the transducer geometry allow defining directly the PSF.

  Along the axial propagation direction, the pulse emitted by the probe, and so the PSF, is defined as a sine wave modulated by a Gaussian with standard deviation σ_{ax}. This

pulse is the impulse response of a bandwidth filter which has, in the frequency domain, a Gaussian shape centered on the pulse frequency. From this shape assumption, it is possible to deduce directly σ_{ax} from the pulse emission spectrum quality factor Q (which is one of the probe parameters) and the wavelength λ by:

$$\sigma_{ax} = \frac{\lambda \cdot Q \cdot \sqrt{\ln(2)}}{\pi} \tag{9}$$

The constant ultrasonic field assumption is no more respected. The ultrasonic field spatial variation is modeled by the PSF spatial variation. The beam expansion has been linearly simulated as following:

$$\sigma_{lat}(y) = \sigma_{lat}(0) + k_1 \cdot y$$
$$\sigma_{trans}(y) = \sigma_{trans}(0) + k_2 \cdot y \tag{10}$$

$\sigma_{lat}(0)$ and $\sigma_{trans}(0)$ are deduced directly from the transducer geometry (the Gaussian full width half maximum FWHM of $\sigma_{lat}(0)$ and $\sigma_{trans}(0)$ has been set, respectively, to the width and height of the transducer) and k_1 and k_2 from the ultrasound propagation physics. The PSF is also described within the polar coordinate system. This transform also depends on it spatial location.

3 Results and discussion

3.1 Methodology implementation

In order to validate our framework, we propose to simulate hepatic US images obtained by the classical probes used by physicians. For this, the radiologist acquired first an injected CT clinical abdominal volume (slices of 1024x1024 pixels, the pixel resolution is 0.68 mm with a slice thickness of 3 mm and an interslices spacing of 15 mm) from a patient. For comparison, on the same patient, the radiologist acquired right intercostal US images with a C2 5 circular ultrasound scanning 3.5 MHz probe in a position as closed as possible to the CT slices location.

This circular probe is a 128 transducers curved array with a curvature radius of 40 mm that geometrically steers to a maximum sector angle of 60 degrees. This geometry is simulated

in the CT volume coordinate system. The user has the choice of the probe position and orientation. The simulated pulse frequency is 3.5 MHz with a Q quality factor of 10 ($\sigma_{ax} \approx 3 \cdot \lambda$).

The tissue acoustical impedances of the several organs have been found in the literature. They have been set to 0.0004, 1.35, 1.65 and 5 10^6 kg $\cdot$ m$^{-2} \cdot$ s^{-1} for respectively air, fat, soft tissues and bone. The definition of the scatter model density and shape parameters (Equation 8) was more problematical. In our knowledge, any study has been performed in order to identify these parameters on US images of the several organs. In order to validate our model, we assigned some ad hoc chosen tissue scatter model density and shape parameters according to some prior knowledge on the scatterers organization. For example, water and air have a low density of irregular arranged scatterers ($1/\overline{d} = 0.002\lambda$ and $\alpha = 0.1$); fat has a high density of regular arranged scatterers ($1/\overline{d} = 0.1\lambda$ and $\alpha = 10$) and liver presents medium density and regularity ($1/\overline{d} = 0.08\lambda$ and $\alpha = 0.4$).

All the computation processes have been developed using the C++ language and implemented on a standard PC (Pentium4 CPU 3.2 GHz, 1Go RAM).

The figure 1 presents the steps of the US image simulation processing.

Figure 1-a: the CT scan image. The beam position and the simulated ultrasound image final geometry have been enhanced. The target organs are the liver and the stomach (see annotation of Figure 4).

Figure 1-b: the tissues' classification. This map is obtained after segmentation of the previous image in several classes (bone, soft tissues, water and fat).

Figure 1-c: the acoustical impedance map. The enhanced part of the CT image is transformed from Cartesian to polar coordinate system. The image has been resampled along the propagation direction in order to respect Shannon's sampling theorem. For f=3.5 MHz (λ=0.44 mm) and a 0.68 mm pixel size, an interpolation ratio of 4 has been chosen. The tissue acoustical impedances are assigned to the map according to the tissues' classes and the speckle texture modeling the micro-inhomogeneities. The impedances are represented as gray level on the figure.

Figure 1-d: the resulting radiofrequency image. On Equation 5, the second order derivate

along the propagation axis of the acoustical impedance map Z_{3D} is problematic to perform because this later is composed by point scatterers. The convolution described in Equation 5 has been transformed as: $I(x,y) = (\frac{\partial^2 H_{3D}}{\partial y^2} * Z_{3D})(x,y,z_0)$ in order to compute the resulting radiofrequency image. This image has been normalized in the figure.

Figure 1-e: the RF image envelop detection. The RFimage is considered as the envelop real part, its imaginary part is estimated using the Hilbert transform. The final image is the magnitude of this complex.

Figure 1-f: the final simulated ultrasound image after back transformation to the Cartesian coordinate system. The final has a size of 1200x1200. The computing time of this image is around 6 seconds on the PC.

The influence of some simulated probe parameters has also been tested :

- Pulse frequency influence: this influence can be seen in figure 2. The image on the left has been simulated with a pulse frequency of 1 MHz, the other on the right with a pulse frequency of 5 MHz. The influence of the pulse frequency on the spatial resolution can be easily seen on the images: the higher the pulse frequency, the higher the spatial resolution. In these simulations we did not take care on the signal attenuation caused by tissues' absorption (cf. discussion).

- Probe influence: in figure 3, two images have been produced by the simulation of two probes having the same size and pulse frequency but one with 64 elements and the other with 128 elements. The number of elements and their size have a direct impact on the lateral resolution of the simulated images.

3.2   Real and simulated US images comparison

We compared qualitatively the real abdominal US images with the simulated ones. In both cases the pulse frequency was 3.5 MHz. The simulated probes were set on the CT slices as close as possible as the real US probe position. In Figure 4, simulated US images (on the right) are compared to the corresponding real ones (on the left). On these images, the mutual characteristics of both images but also the disparities between our model and a real US image can clearly been outlined.

11

Qualitatively, we find in the simulated US image some of the main characteristics of a real US image:

- The simulated US image is mainly produced by speckle patterns which are organized on concentric circles. The speckle size grows laterally when the distance from the probe increases.

- The simulated speckle organization is relatively similar to the real one for each kind of tissues. This produces simulated images with speckle characteristics relatively close to the real images (fat, vessels, etc.).

- The acoustical interface between tissues is well delineated as in real images.

- The pulse frequency and the number of probe transducers seem to have the expected behavior on the simulation. Higher pulse frequencies give finer speckle in the axial direction and so enhance the spatial image resolution. A high number of transducers provides finer speckle in the lateral direction.

In the Introduction we state that the final aspect of an US image is mainly provided by the speckle distribution. The previous results validate this assumption. But, the tissue micro-inhomogeneities model can still be improved in order to enhance the realism of the simulated image. The next improvement of our model should be the identification of the tissue scatter model density and shape parameters from real US images.

However, other US image characteristics have not been taken into account. This is the case for example of the signal attenuation by the medium absorption: the amplitude change of a decaying wave can be expressed as $A = A_0 \exp(-\alpha x)$ where A_0 is the unattenuated amplitude of the propagating wave and α the attenuation coefficient. US devices compensate this attenuation by amplification with a gain increasing exponentially with the depth. This gain has the effect to enhance the attenuated signal but also the noise. In our simulation, this gain could be simply modeled by a Gaussian noise with a magnitude and a standard deviation increasing exponentially with the distance to the probe. More generally, the US device manufacturer handles the raw signals and the images during the acquisition by some hidden processing. This device processes explain some of the aspect differences between the

simulated and the real images (range normalization smoothing, etc.) but could be difficult to correct explicitly.

Other US image characteristics like acoustic shadow or mirror effect are totally absent from the simulated images. This comes directly from the used model where the wave propagation and reflection are not simulated explicitly; however, these effects are generally considered as artifacts on the real US images.

But beyond these remarks, additional differences between simulated and real images remain. We have not taken the operators pressure on the probe and the resulting organs' deformation into account. Apart from the simulated probe mislocation, the pressure can explain some morphologic changes between the real and the simulated images.

The simulation computer time is short in comparison to other simulation approaches (a few seconds on a classical PC). Moreover, the use of specialized signal processing or mathematical libraries or vector processors could accelerate the computation speed in order to produce an image within the video refreshing time interval.

4   Conclusions

This study presents the first results of an abdominal US image simulation. The model proposed by Bamber and Dickinson has been efficiently adapted to a high field of view US image simulation obtained by a circular probe. These simulations have been obtained in a fairly fast computation speed and qualitatively they present most of the real US images main characteristics: influence of the number of transducers and US frequency, speckle position and shape, acoustical interface between tissues, etc.

References

[1] J. A. Jensen. Field: a program for simulating ultrasound systems. *Med Biol Eng Comput*, 34:351–353, 1996.

[2] A. P. Berkhoff, J. M. Thijssen, and R. F. Homan. Simulation of ultrasonic imaging with linear arrays in causal absorptive media. *Ultrasound Med Biol*, 22:245–256, 1996.

[3] J. Meunier and M. Bertrand. Ultrasonic texture analysis: theory and simulation. *IEEE Trans Med Im*, 14(2):293–300, 1995.

[4] M. Sühling, M. Arigovindan, C. Jansen, P. Hunziker, and Unser M. Myocardial motion analysis from B-mode echocardiograms. *IEEE Trans Im Process*, 14(4):525–536, 2005.

[5] O. Aiger and D. Cohen-Or. Real-time ultrasound imaging simulation. *Real-Time Imaging*, 4(4):263–274, 1998.

[6] J. Troccaz, D. Henry, N. Laieb, G. Champleboux, J.-L. Bosson, and O. Pichot. Simulators for medical training: application to vascular ultrasound imaging. *The Journal of Visualization and Computer Animation*, 11(1):51–65, 2000.

[7] R.M. Cramblitt and K.J. Parker. Generation of non-Rayleigh speckle distributions using marked regularity models. *IEEE Trans Ultrason Ferroelectr Freq Control*, 46(4):867–874, 1999.

[8] P. M. Shankar. The use of the compound probability density function in ultrasonic tissue characterization. *Phys Med Biol*, 49(6):1007–1105, 2004.

[9] S. Nadarajah. Statistical distributions of potential interest in ultrasound speckle analysis. *Phys Med Biol*, 52(10):N213–N227, 2007.

[10] J. A. Jensen and S. I. Nikolov. Fast simulation of ultrasound images. In *Proc. of IEEE Int. ultrasonic Symp.*, pages 1721–1724, Puerto Rico, 2000.

[11] J. C. Bamber and R. J. Dickinson. Ultrasonic B-scanning: a computer simulation. *Phys Med Biol*, 25:463–479, 1980.

[12] C. Laporte, J. Clark, and T. Arbel. A fractal multi-dimensional ultrasound scatterer distribution model. In *IEEE Int. Symp. on Biomedical Imaging*, pages 880–883, Washington D.C., 2007.

[13] J. J. Bartholdi III and P. Goldsman. Vertex-labeling algorithms for the Hilbert space-filling curve. *Software: Practice and Experience*, 31(5):395–408, 2001.

[14] S. Laguitton, J.-J. Patard, and J.-L. Dillenseger. Fast simulation of ultrasound images from a CT volume. In *EMBEC'05*, volume 11, page 4 pages, Prague, 2005.
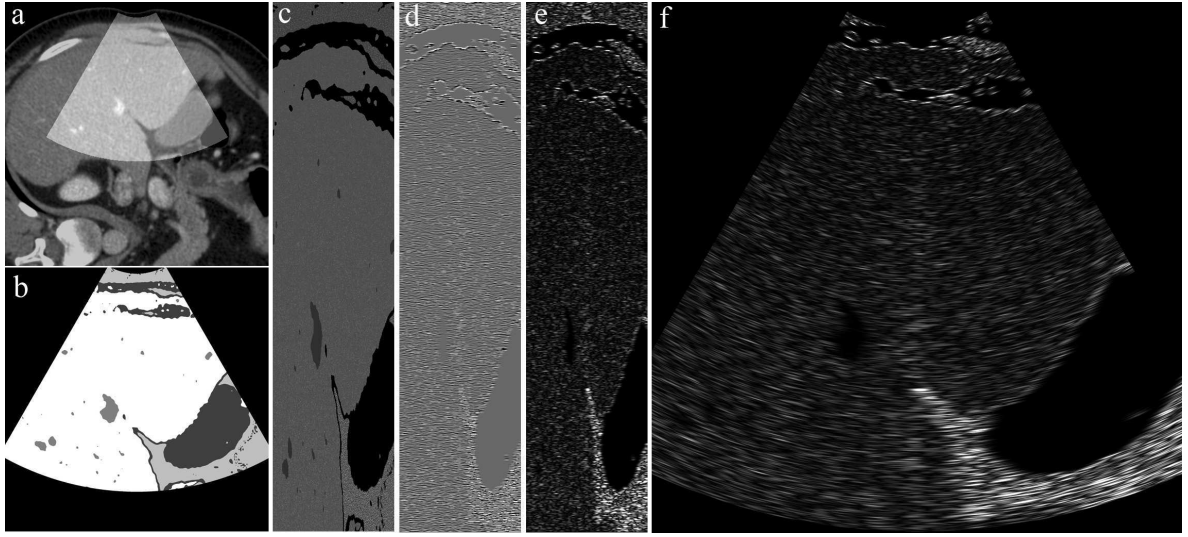
List of Figures

Figure 1: Ultrasound image simulation: a) CT image, the simulated zone is enhanced; b) tissue classification; c) acoustical impedance map after polar transformation and resampling, this map corresponds to the zone highlighted in a); d) radiofrequency image after convolution of acoustical impedance map with the PSF; e) radiofrequency image envelop detection calculated with the Hilbert transform; f) simulated ultrasound image after polar/Cartesian transformation.
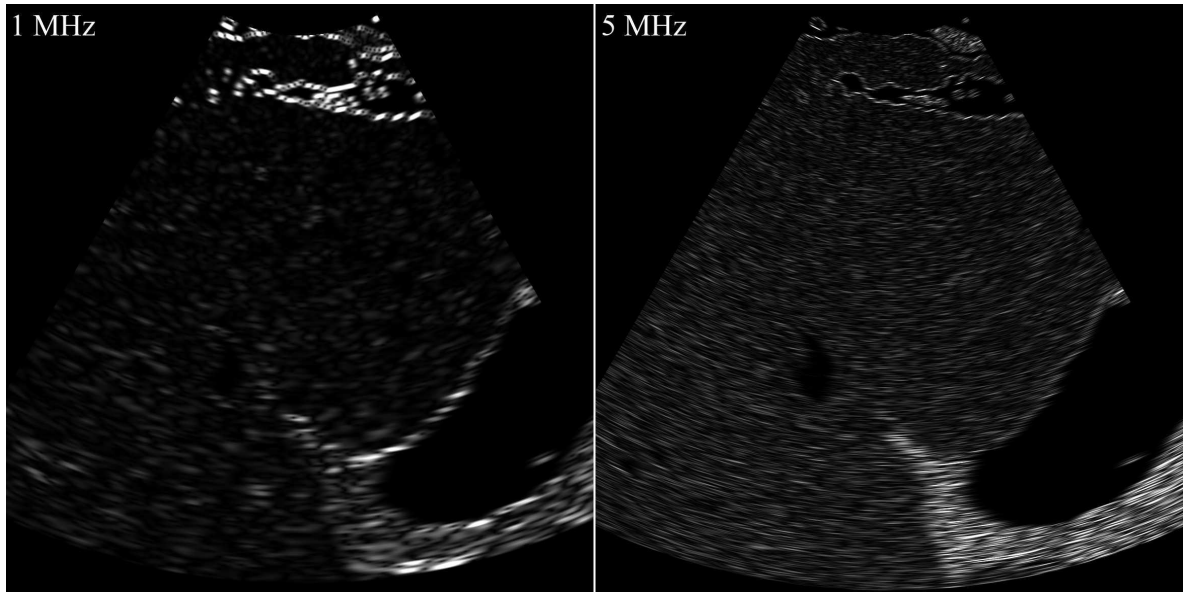
Figure 2: Influence of the pulse frequency. Ultrasound image simulations with a pulse frequency of 1 MHz (left) and of 5 MHz (right).
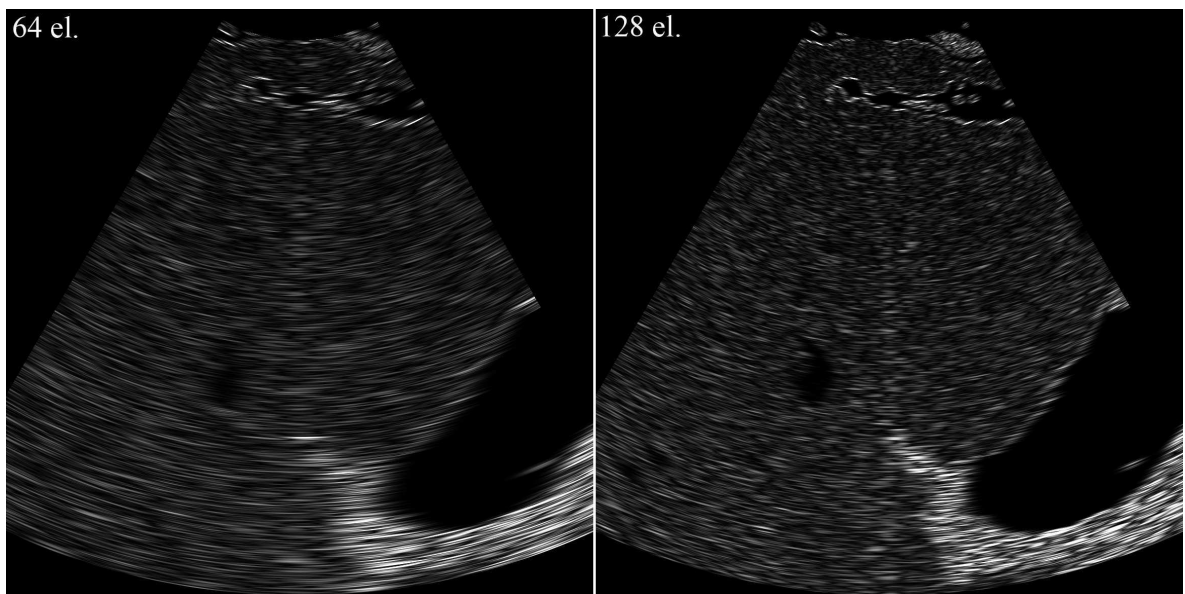

Figure 3: Influence of the probe geometry. Two 3.5 MHz ultrasound image simulations with a 64 (left) and a 128 elements probe (right).
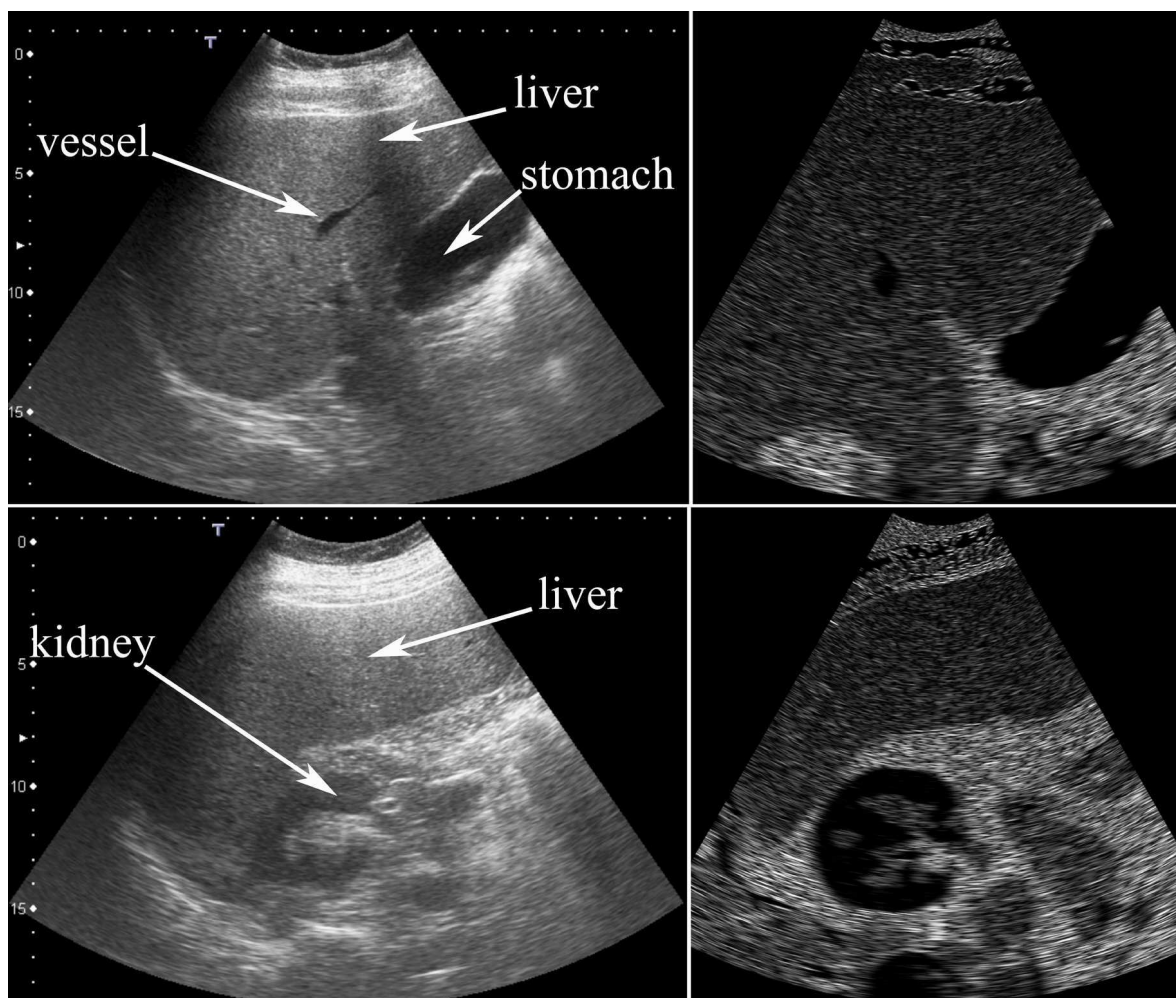
Figure 4: Comparison between two real 3.5 MHz ultrasound images (left) and the simulated ones (right).